ACS Photonics

Letter

pubs.acs.org/journal/apchd5

Enhanced Quantum Dot Spontaneous Emission with Multilayer Metamaterial Nanostructures

Ling Li,[†] Wei Wang,[†] Ting S. Luk,[‡] Xiaodong Yang,[†] and Jie Gao*[,†]

[†]Department of Mechanical and Aerospace Engineering, Missouri University of Science and Technology, Rolla, Missouri 65409, United States

[‡]Center for Integrated Nanotechnologies, Sandia National Laboratories, Albuquerque, New Mexico 87185, United States

Supporting Information

ABSTRACT: The Purcell effect of quantum dot (QD) spontaneous emission with Ag-SiO_2 multilayer metamaterial nanostructures has been demonstrated in experiment and simulation. A broadband enhanced spontaneous emission rate of QDs is observed due to large local density of states in the epsilon-near-zero and hyperbolic regions of multilayer structures. Multilayer gratings are utilized to further enhance the QD spontaneous emission as the QDs located inside the grating grooves strongly interact with high-*k* coupled surface plasmon polariton modes. Photoluminescence decay measurements are in good agreement with both analytical treatment with a nonlocal effect and three-dimensional finite-element simulation. Detailed studies of QD position and polarization effects on emission rate enhancement for multilayer and multilayer grating nanostructures provide important insight for understanding the coupling mechanisms of emitter−multilayer interaction and the engineering of local density of states in metamaterial nanostructures. These results will advance many applications in light-emitting devices, nanoscale lasers, quantum electrodynamics, and quantum information processing.

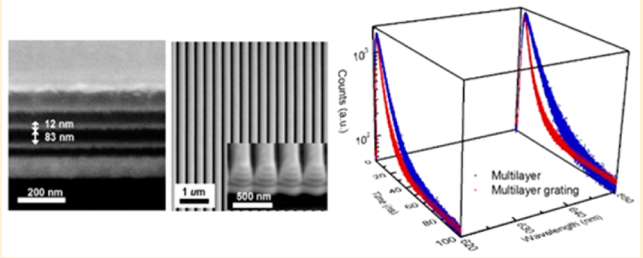

KEYWORDS: *metamaterials, quantum dots, Purcell effect, spontaneous emission enhancement, light−matter interaction*

Multilayer metamaterials consisting of alternating subwavelength layers of a metal and a dielectric have been studied extensively in recent years. The periodic spatial layout of metal and dielectric layers makes multilayer metamaterials artificial uniaxial anisotropic materials with unique optical properties compared with their counterparts in nature. Electromagnetic waves propagating through them undergo a transition from closed elliptical to open hyperbolic dispersions when one or two principle components of the permittivity tensor pass through zero at specific wavelengths. At these wavelengths, the appearance of ultralong wavelengths accompanying epsilon-near-zero (ENZ) behaviors of electromagnetic waves manifests as extreme slow phase modulation, which is highly desirable in wavefront shaping and directional emission.[1−6] In the hyperbolic region of the multilayer metamaterials, optical modes with anomalously large wave vectors enabled by coupled surface plasmon polaritons (SPPs) on metal−dielectric interfaces provide tremendous capabilities of near-field subwavelength imaging and large local density of states (LDOS) for spontaneous emission rate enhancement.[3,5,7−17] The wide tunability of the anisotropic optical property by changing the metal filling ratio and layer thickness leads to broad applications for multilayer metamaterials.[3,5,18]

Spontaneous emission enhancement is very important for advances in single-photon sources, light-emitting devices, low-threshold photonics, and plasmonic lasers. Among many systems, microcavities and photonic crystals have been extensively studied for spontaneous emission rate enhancement by the cavity Purcell effect.[19,20] They provide a high resonant quality factor, tight electromagnetic field confinement, and thus large spontaneous emission rate enhancement. However, the resonant requirement limits the spectral bandwidth for the cavity Purcell effect, hindering the broadband emission operation. This resonance requirement also exists in a parallel line of studies on spontaneous emission rate enhancement using plasmonic nanostructures such as nanoparticles and nanoantennas.[21−23] The coupling strength between an emitter and the plasmonic resonant mode is enhanced due to the subwavelength mode volumes of plasmonic nanostructures. Compared to all these resonant structures with narrow spectral widths and spatially localized electromagnetic modes, planar multilayer metamaterial nanostructures are capable of providing broadband Purcell effects on spontaneous emission. In the hyperbolic dispersion regime, these multilayer metamaterials possess ideally divergent LDOS, leading to very large Purcell factors in the broadband.[9,16,17]

Various hyperbolic multilayer metamaterials have been used to enhance spontaneous emission of fluorescent emitters such as dye molecules and QDs.[10,11,15,17,24] Subwavelength gratings were also fabricated in multilayer structures to further couple spontaneous emission to high wave vector modes inside those

Received: December 27, 2016
Published: March 2, 2017

DOI: 10.1021/acsphotonics.6b01039
ACS Photonics 2017, 4, 501−508

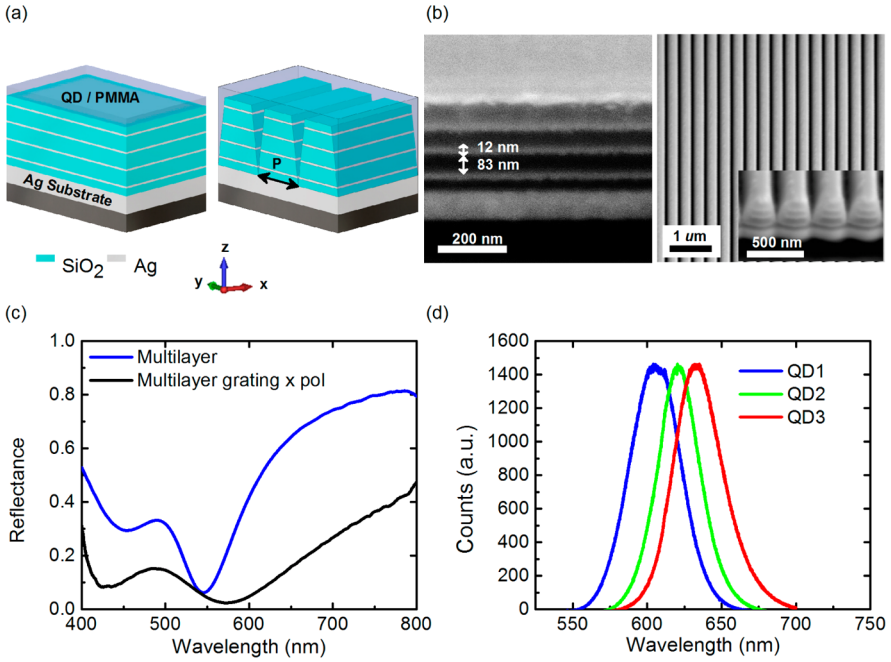

Figure 1. Multilayer metamaterial nanostructures. (a, b) Schematic and SEM for a multilayer structure and multilayer gratings. The multilayer is composed of four pairs of Ag layers (thickness a_m = 12 nm) and SiO_2 layers (thickness a_d = 83 nm), with unit cell thickness $a = a_m + a_d$ = 95 nm and a total thickness of 380 nm. The multilayer is deposited on the 100 nm Ag substrate as a reflector. A multilayer grating nanostructure with a grating period P = 300 nm is fabricated, and the bottom angle of the grating groove trapezium is 82.5°. A thin layer of QDs in PMMA is spin-coated on the surface of the multilayer nanostructures. (c) Reflection spectra of a multilayer and multilayer gratings. (d) Emission spectra of the three sets of CdSe/ZnS QDs on a glass substrate.

hyperbolic multilayer metamaterials.[15,17,24,25] In these studies, an effective medium theory (EMT) approximation is normally employed to predict the ENZ wavelength and calculate the Purcell factor, guiding the design of multilayer metamaterials for tunable spontaneous emission enhancement. However, without the consideration of nonlocal effects of multilayers, it is not able to fully predict or explain the measurements on the ENZ response and Purcell factor of multilayer structures.[26−29]

In this work, Ag−SiO_2 multilayer metamaterial and multilayer grating nanostructures are utilized to realize a 3- to 6-fold enhanced spontaneous emission rate of CdSe/ZnS QDs in a broad wavelength range from 570 to 680 nm. For a multilayer structure, a large LDOS in the ENZ and hyperbolic regions results in a higher Purcell factor and QD emission rate enhancement compared to the elliptical region. Multilayer gratings facilitate the positioning of QDs inside grating grooves and strengthen the QDs' interaction with high-k coupled SPP modes so that the spontaneous emission rate is further enhanced. Time-resolved fluorescence experiments are performed to measure emission rate enhancement, which are in good agreement with theoretical analysis and numerical simulation based on actual multilayer parameters. Moreover, we investigate the spatial and polarization dependence of emission rate enhancement, as well as the electric field distributions excited by dipole emitters. It is revealed that the z-polarized dipole dominates the emission rate enhancement on a multilayer surface due to the coupling with an SPP wave, while a y-polarized dipole possesses a large emission rate enhancement inside grating grooves due to the strong excitation of high-k coupled SPP modes in the multilayer gratings (see coordinates in Figure 1a). The results pave the way to the understanding of enhanced light−matter interactions between quantum emitters and metamaterial nanostructures, as well as the advancement of metamaterial-based applications in light-emitting devices, nanoscale lasers, optical sensing, quantum electrodynamics, and quantum information processing.

RESULTS AND DISCUSSION

Figure 1a shows a schematic of the Ag−SiO_2 multilayer metamaterial and multilayer grating nanostructures. The multilayer consists of four alternating pairs of Ag and SiO_2 layers, with the designed layer thickness of a_m and a_d for Ag and SiO_2, respectively. A half-layer of SiO_2 is deposited as top and bottom layers in order to achieve symmetric multilayer structures and also to protect the Ag layer from oxidizing. The filling ratio of Ag, $f_m = a_m/a$, where $a = a_m + a_d$ is the multilayer unit cell thickness, can be chosen to achieve spontaneous emission rate enhancement within specific wavelength range. Subwavelength gratings are designed on the multilayer with a grating period P = 300 nm. A thin layer of QDs in poly(methyl methacrylate) (PMMA) is spin-coated on the surface of multilayer nanostructures. Scanning electron micrographs (SEM) of a multilayer and multilayer gratings are shown in Figure 1b. The left panel shows the cross-section view of the multilayer structure, where Ag and SiO_2 layers are visible as bright and dark bands, with layer thicknesses of 12 nm (a_m) and 83 nm (a_d), respectively. These layer thicknesses are obtained by fitting the multilayer reflection spectrum using the transfer-matrix method (see Figure S1, Supporting Information). The right panel of Figure 1b shows a top-view SEM of periodic gratings fabricated in the multilayer structure with multilayer ridges (bright color) and air grooves (dark color). The inset shows a tilted-view SEM of a multilayer grating where individual layers are also clearly presented. The permittivity of Ag and SiO_2 layers is also characterized during the multilayer

DOI: 10.1021/acsphotonics.6b01039
ACS Photonics 2017, 4, 501−508

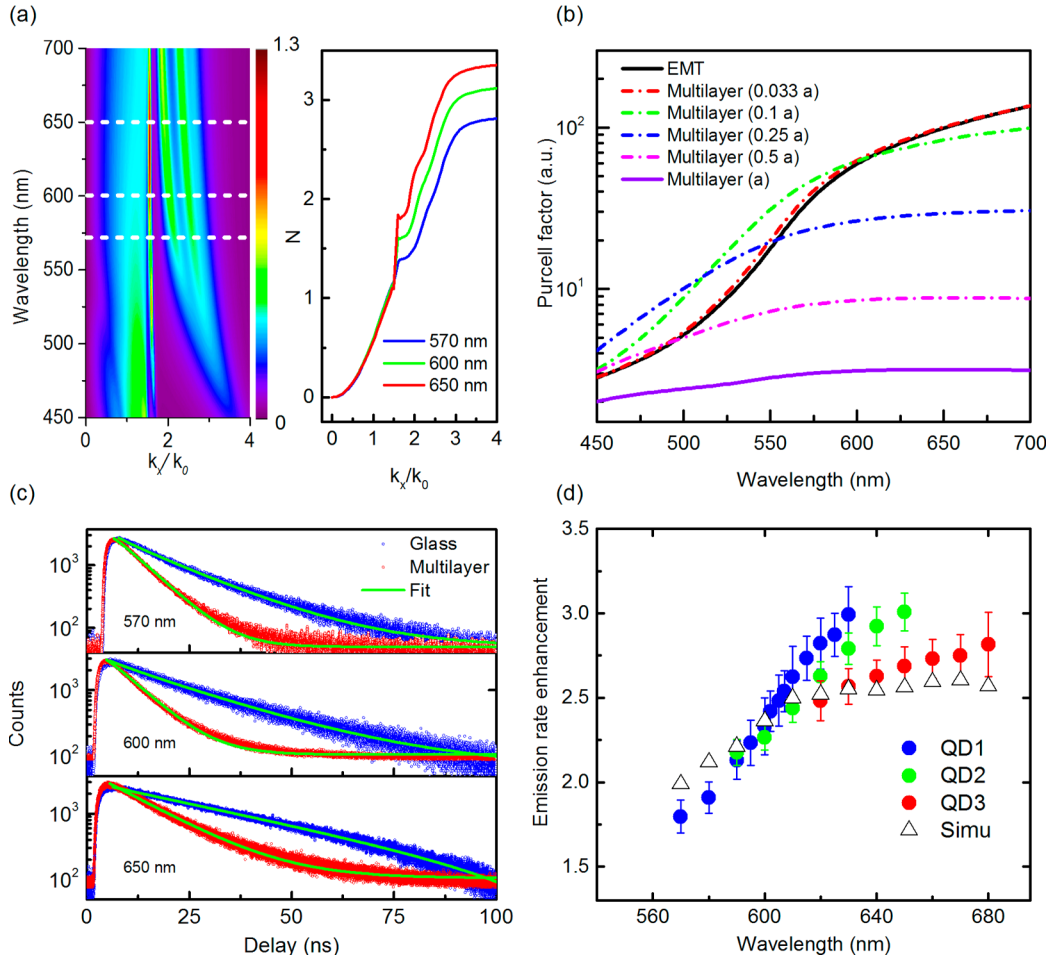

Figure 2. Spontaneous emission enhancement of QDs on a multilayer structure. (a) Left: normalized dissipated power spectrum (intensity on a logarithmic scale) for dipole emission at a distance of 10 nm above the multilayer surface; right: cumulative LDOS of dipole emission at wavelengths of 570 nm (elliptical), 600 nm (ENZ), and 650 nm (hyperbolic), as denoted by the three white dashed lines in the left panel. (b) Theoretical Purcell factor calculations for multilayer metamaterials with varying unit cell thickness and EMT approximation. (c) Photoluminescence decay measurements for QD emission on glass (blue circle) and the multilayer (red circle) at wavelengths of 570, 600, and 650 nm. The green lines are a theoretical fitting using a modified exponential model. (d) QD emission rate enhancement shown in dots by normalizing the QD photoluminescence decay lifetime obtained from the measurements on the glass substrate with that on the multilayer sample and 3D simulation results of the emission rate enhancement shown as hollow triangles.

deposition process (see Figure S2). The reflection spectra of both a multilayer and multilayer gratings are shown in Figure 1c. The multilayer ENZ wavelength retrieved using nonlocal EMT based on the transfer-matrix method is at 600 nm, vastly different from 561 nm, which is derived by local EMT (see Figure S3). Figure 1d shows the photoluminescence spectra of three sets of CdSe/ZnS QDs, with center emission wavelengths of 604 nm (QD1), 620 nm (QD2), and 630 nm (QD3), respectively. They provide a broadband emission wavelength range spanning from 550 to 700 nm to ensure probing the Purcell effect of QD emission in elliptical, ENZ, and hyperbolic regions of the multilayer metamaterial nanostructures.

In order to understand the LDOS and Purcell effect of the multilayer metamaterial, we first investigate the Purcell factor of the multilayer theoretically based on the multilayer parameters in the fabricated sample. Figure 2a shows the normalized dissipated power spectrum and the accumulated LDOS enhancement of an electric dipole 10 nm above the multilayer surface. The theoretical normalized dissipated power spectrum in the left panel is obtained by averaging two orthogonal polarizations to estimate the random dipole orientation in the experiment, i.e., $\frac{1}{3}\frac{dP_\perp}{dk_x} + \frac{2}{3}\frac{dP_\parallel}{dk_x}$ (see Methods section for more details). To show that the LDOS of the multilayer structure evolving from elliptical to hyperbolic dispersion regions cross the ENZ wavelength, the right panel of Figure 2a compares the cumulative LDOS, $N(u) = \int_0^u \left(\frac{1}{3}\frac{dP_\perp}{dk_x} + \frac{2}{3}\frac{dP_\parallel}{dk_x}\right)du$, at emission wavelengths of 570, 600, and 650 nm, as correspondingly marked as three white dashed lines in the left panel, where $u = k_x/k_0$ is the normalized wave vector component parallel to multilayer surface. It is shown that the dipole emitter couples almost equally to the low-k propagation modes at the three wavelengths, but interacts with the high-k coupled SPP modes existing at the multilayer interfaces with much stronger coupling strengths in the ENZ and hyperbolic regions (600 and 650 nm), resulting in higher dissipated power and larger LDOS compared to the elliptical region (570 nm). Figure 2b shows the theoretical prediction of the Purcell factor for QD emission on the surface of a multilayer structure with a = 95 nm (purple solid curve), which gives an average Purcell factor of 2.5. The influence of the multilayer unit cell thickness on the

DOI: 10.1021/acsphotonics.6b01039
ACS Photonics 2017, 4, 501−508

Purcell factor is examined with decreasing the unit cell thickness but fixing the Ag filling ratio, as shown by the dashed curves in Figure 2b. It demonstrates that smaller unit cell thickness leads to a larger Purcell factor due to stronger couplings between SPPs on metal−dielectric interfaces and higher cutoff wave vectors in the integration of LDOS. When the multilayer unit cell thickness is deceased to infinitely small, the calculated Purcell factor approaches the result based on EMT (black solid curve). It is worth noting that the EMT approximation overestimates the Purcell factor of QD emission on an actual multilayer structure because EMT ignores the finite layer thickness and includes infinitely large wave vector modes contributing to the Purcell factor 1 order of magnitude higher. The Purcell factors for QD emission on the Ag−SiO_2 multilayer with various Ag filling ratios at a fixed unit cell thickness are also illustrated in Figure S4.

To demonstrate the Purcell effect of a metamaterial multilayer, time-resolved photoluminescence decay measurements of QDs on a multilayer and glass (control) are conducted (see the Method section). Figure 2c presents the photoluminescence decay data from QDs on the multilayer at emission wavelengths of 570, 600, and 650 nm, which show faster decay than that on the glass substrate. It is also observed that the QD spontaneous emission lifetime at wavelengths of 600 and 650 nm is shorter compared to that at 570 nm, indicating a stronger Purcell effect in the ENZ and hyperbolic regions. QD concentration and laser excitation power are carefully controlled in these experiments at an extremely low level to make sure the observed photoluminescence decays are very close to single-exponential decays. All the decay curves at different emission wavelengths are fitted using a modified exponential relaxation model (see the photoluminescence decay curve fitting in the Methods section).[30−33] The fitted decay times for these curves of QDs on the multilayer (glass) in Figure 2c are 7.91 (14.44) ns at 570 nm, 8.27 (19.35) ns at 600 nm, and 12.79 (34.10) ns at 650 nm. Figure 2d illustrates the emission rate enhancement of the multilayer structure as a function of wavelength, which is obtained by normalizing the QDs' photoluminescence decay lifetime on the glass substrate with that on the multilayer sample. The error bar at each wavelength reflects the variation of the measured lifetime at more than 10 different spots on the sample surfaces. It is shown that the emission rate enhancement from all three sets of QDs covering a broad wavelength range increases from the elliptical to the hyperbolic dispersion region of the multilayer structure. There is some discrepancy of the measured emission rate enhancement between different sets of QDs especially at the longer wavelengths, due to different number densities, optical and chemical environment, and size distribution of QDs originating from the synthesis process. The emission rate enhancement is also modeled with three-dimensional (3D) finite-element simulation using the geometric and material properties as detailed in Figure 1. The simulation takes into account the dipole position, polarization, and quantum efficiency effects on emission rate enhancement as a function of wavelength.[11,17,34,35] The simulation results (hollow triangles in Figure 2d) are averaged from 10 vertical dipole positions and three orthogonal polarizations for each emission wavelength (see Methods section), which show excellent agreement with the measurements.

To further enhance the interaction between QDs and multilayer metamaterials, a subwavelength grating nanostructure is introduced into the multilayer to provide larger spatial overlap and enable stronger coupling between QDs inside the grating grooves and the high-k SPP mode of the multilayer structure.[17,24] Representative photoluminescence decays of QDs at two emission wavelengths measured on a multilayer and multilayer gratings are shown in Figure 3a. We observe that data from both nanostructures can be fitted by the modified exponential decay model very well, and QDs on multilayer

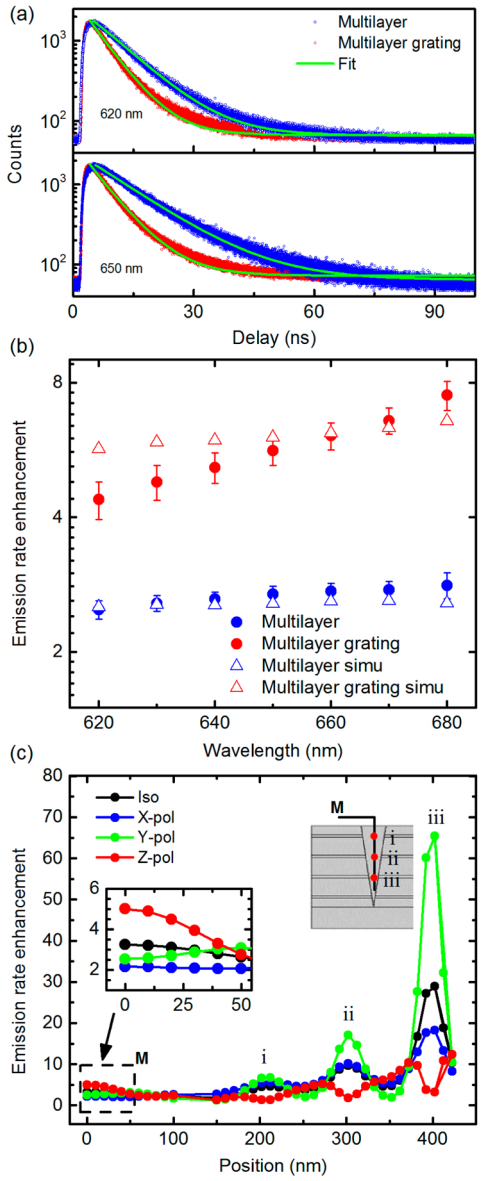

Figure 3. Spontaneous emission enhancement of QDs on multilayer gratings. (a) Photoluminescence decay measurements for QD emission wavelengths at 620 and 650 nm on a multilayer (blue circle) and a multilayer grating (red circle). (b) Emission rate enhancement obtained by normalizing the measured QDs' photoluminescence decay lifetime on a glass substrate with that on multilayer nanostructures shown by dots, together with the 3D simulation results averaging from different dipole positions and polarizations on the nanostructures. (c) Simulation of emission rate enhancement for x-, y-, and z-polarized dipole emission at 620 nm at various locations and the average of three polarizations, labeled as Iso. The x-axis represents the distance starting from the grating ridge center (M point) to all the positions along the black line toward the grating groove bottom (shown in the inset schematic).

DOI: 10.1021/acsphotonics.6b01039
ACS Photonics 2017, 4, 501−508

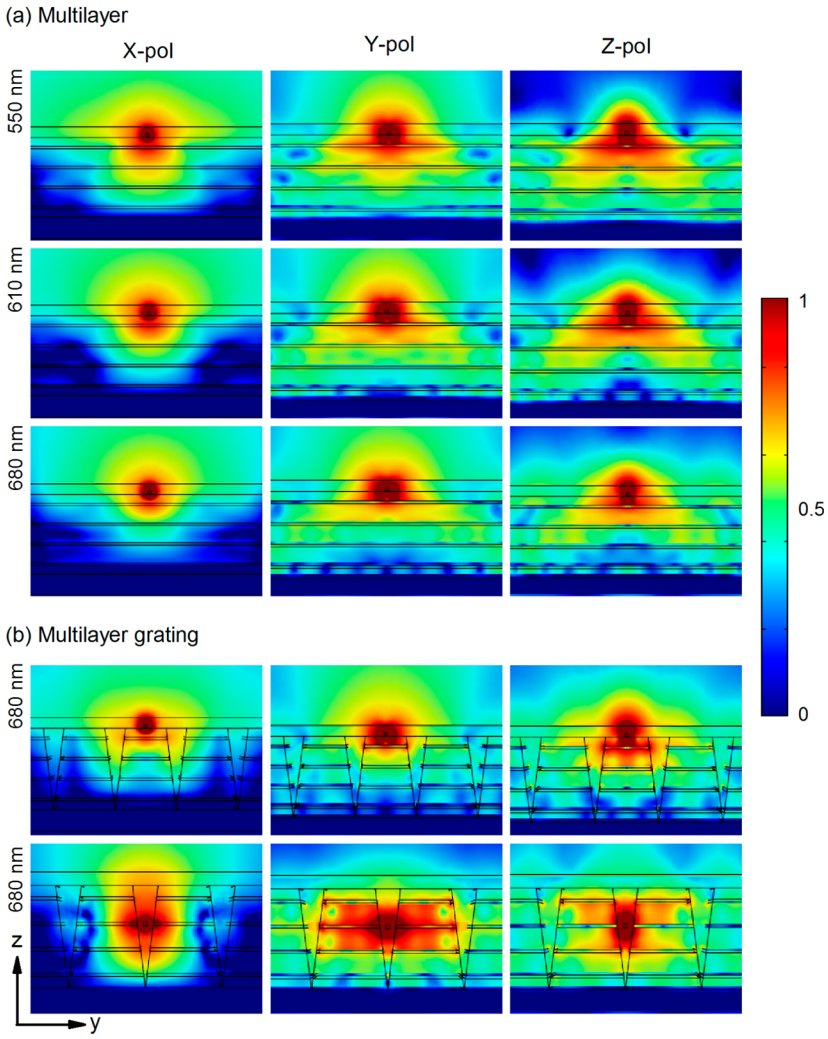

Figure 4. Simulated electric field magnitude distribution of QDs with emission wavelengths of 550, 610, and 680 nm on top of a multilayer (a) and at 680 nm on and inside a multilayer grating (b). Three columns of electric field distributions are from dipole emission with *x* polarization (X-pol), *y* polarization (Y-pol), and *z* polarization (Z-pol), respectively.

gratings have shorter decay times compared to QDs on a multilayer. The fitted decay times for these curves of QDs on a multilayer grating (multilayer) in Figure 3a are 6.11 (9.97) ns for 620 nm and 6.53 (12.79) ns for 650 nm. Subsequently, emission rate enhancement of a multilayer and a multilayer grating structure at all wavelengths covered by QD3 emission is obtained by normalizing the QD photoluminescence decay lifetime on a glass substrate with that on a multilayer and a multilayer grating, denoted by solid dots in Figure 3b, together with the well-matching 3D finite-element simulation results (solid lines). The spatial and polarization dependence of the emission rate enhancement are also investigated by simulation of dipole emission at different locations on a multilayer grating as depicted in Figure 3c. The position axis measures distances from the QD site 10 nm above the center of a grating ridge surface toward the grating groove surface and then down to the grating groove bottom, as illustrated by the black line in the schematic inset of Figure 3c. The red dots on that curve denote three QD locations (i, ii, iii) inside the grating groove at the position of silver layers, and correspondingly three peaks in emission rate enhancement are observed with strong Purcell effects at these locations. Moreover, emission rate enhancement shows different dipole polarization dependence when the emitter is located on the top of the grating surface and at the bottom of the grating groove. When a QD emitter is located at the grating ridge center, the contribution from *z*-polarization dominates the averaged emission rate enhancement over *x*- and *y*-polarization because the SPP wave in the multilayer structure can be excited well by the *z*-polarized dipole. When the emitter resides in positions (i, ii, iii) inside the groove, emission rate enhancement for the *y*-polarized dipole shows a large Purcell effect due to the strong excitation of the high-*k* coupled SPP modes in the multilayer gratings. Additionally, as the groove width shrinks, the coupling gets even stronger, leading to the significantly increased emission rate enhancement at position (iii).

To show more clearly the influence of an emitter's positions and polarizations on the Purcell effect of multilayer metamaterial nanostructures, electric field distributions of a dipole emitter 10 nm above the multilayer surface and inside the multilayer grating groove are illustrated in Figure 4. Figure 4a shows electric field magnitude distributions inside a multilayer at three emission wavelengths, 550, 610, and 680 nm, to demonstrate the increasing LDOS for a dipole emitter on top of a multilayer surface from the elliptical to the hyperbolic dispersion region. The third column of Figure 4a

DOI: 10.1021/acsphotonics.6b01039
ACS Photonics 2017, 4, 501−508

shows that the *z*-polarized dipole strongly couples to the multilayer and contributes mostly to the Purcell factor. As emission wavelength moves from the elliptical to the ENZ and hyperbolic regions, the electric fields from dipole emission penetrate deeper into the multilayer. Figure 4b presents the electric field magnitude distribution from an emitter with an emission wavelength at 680 nm on top of and inside the groove of a multilayer grating structure. The electric field intensity distributions of *x*-, *y*-, and *z*-polarized dipole emission in Figure 4b correspond to the emission rate enhancement results shown in Figure 3c. It is noteworthy that inside the grating groove *y*-polarized dipole emission efficiently excites the high-*k* coupled SPP modes across all the metal−dielectric interfaces in the grating nanostructures (as shown in the middle plot of the bottom row in Figure 4b), indicating the enhanced dipole−multilayer coupling with the *y*-polarized dipole which provides the major contribution to the high emission rate enhancement inside the grating groove.

CONCLUSION

We have demonstrated multilayer metamaterial and multilayer grating nanostructures with broadband Purcell effects for CdSe/ZnS QD emission. Several-fold emission rate enhancement is achieved with a large LDOS as the emission wavelength goes from the elliptical to the hyperbolic dispersion regime across the ENZ region of a multilayer metamaterial. Multilayer gratings further enhance the QDs' spontaneous emission as the QDs located inside the grating grooves strongly interact with high-*k* coupled SPP modes. Position and polarization effects on QD emission rate enhancement are studied to reveal the coupling mechanisms and further engineer the LDOS in metamaterial nanostructures. Our results provide insight into the understanding of QD−metamaterial interactions, especially the broadband Purcell effect, LDOS manipulations with different dispersions, and coupling to the high-*k* coupled SPP modes, which have the potential for the development of promising applications in light−matter interactions such as light-emitting devices,[36,37] nanoscale lasers,[38,39] quantum electrodynamics, and quantum information processing.[40,41]

METHODS

Sample Fabrication and Characterization. An electron-beam evaporation system is used to deposit the multilayer stack on silicon substrates at the rate of 0.2 Å/s for both Ag and SiO_2 layers. The designed thickness for the Ag and SiO_2 layer is 10 and 85 nm, respectively. Characterization of the optical constant of each material is performed with a variable-angle spectroscopic ellipsometer (VASE, J. A. Woollam Co. VB400/HS-190). To obtain Ag and SiO_2 layer thickness as denoted in Figure 1, we measure the reflection spectrum of the multilayer under normal incidence and fit it using the transfer-matrix method. The grating on a multilayer is fabricated using focused ion beam milling (FEI Helios Nanolab 600 DualBeam) with a gallium ion current of 9.7 pA and an accelerating voltage of 30 keV. To prepare samples for time-resolved photoluminescence measurements, the original CdSe/ZnS QD solution (QD weight ratio 3%, solvent: chloroform) is diluted with a mixed solution of PMMA (weight ratio 2%, solvent: anisole), anisole, and chloroform, resulting in a final volume ratio of PMMA:anisole:chloroform = 1:3:4 and final weight ratios for QDs and PMMA of 0.05% and 0.2%, respectively. Then the diluted QDs−PMMA solution was spin-coated on surfaces of the multilayer, multilayer grating, and glass samples. The spin lasted for 1 min with a spin speed of 1200 rpm, resulting in one very thin PMMA matrix layer with an estimated thickness of 50 nm.

Theoretical Calculation and Numerical Simulations. QDs are treated as ideal electric dipoles with internal quantum efficiency η. The quantum efficiency for QDs is interpolated as a function of wavelength using experimental values.[35] The Purcell factors experienced by a dipole emitter placed at a distance of d above the planar multilayer with polarization perpendicular ($\perp$) or parallel ($\parallel$) to the multilayer interface are[34]

$$F_{\perp} = 1 - \eta + \eta \mathrm{Re} \int_0^{\infty} \frac{\mathrm{d}P_{\perp}}{\mathrm{d}u} \mathrm{d}u \tag{1}$$

$$F_{\parallel} = 1 - \eta + \eta \mathrm{Re} \int_0^{\infty} \frac{\mathrm{d}P_{\parallel}}{\mathrm{d}u} \mathrm{d}u \tag{2}$$

The two integrands are the normalized dissipated power spectra for the perpendicular and parallel polarizations of the dipole emitter with respect to that of a dipole in a vacuum.[34] In the weak coupling regime, the semiclassical theory is equivalent to the quantum mechanical approach, and the LDOS enhancement and the normalized dipole dissipated power density are equivalent.[12,26,34,42] The corresponding LDOS enhancement is[34]

$$\frac{\mathrm{d}P_{\perp}}{\mathrm{d}u} = \frac{3}{2}\frac{k_0}{k_z}\left(\frac{u}{\sqrt{\varepsilon_1}}\right)^3 [1 + r_p e^{2ik_z d}] \tag{3}$$

$$\frac{\mathrm{d}P_{\parallel}}{\mathrm{d}u} = \frac{3}{4}\frac{k_0}{k_z}\frac{u}{\sqrt{\varepsilon_1}}\left\{1 + r_s e^{2ik_\perp d} + \frac{k_z^2}{\varepsilon_1 k_0^2}[1 - r_p e^{2ik_z d}]\right\} \tag{4}$$

where k_0 is the magnitude of the wave vector in a vacuum, $u = k_x/k_0$ is the wavevector component parallel to the multilayer surface normalized by the vacuum wavevector, $k_z = k_0\sqrt{\varepsilon_1 - u^2}$ is the component of the wavevector perpendicular to the multilayer interface, ∂_1 is the relative permittivity for the host material, PMMA, and $r_{p,s}$ is the reflection coefficient at the interfaces for a p- or s-polarized wave, respectively. In our theoretical calculation, the relative permittivity for PMMA (∂_1) is obtained from a reference, and those for Ag and SiO_2 are from our own characterization data obtained during the fabrication process (see Supporting Information).

All FEM simulations are carried out in COMSOL Multiphysics. A point electric dipole is used to simulate the Purcell factor for a dipole emitter on multilayer nanostructures. Results of the electric dipole with polarization parallel ($PF_{\parallel}$) and perpendicular ($PF_{\perp}$) to the multilayer surface are used to get the average Purcell factor: $PF_{iso} = (1/3)PF_{\parallel} + (2/3)PF_{\perp}$, where $PF_i = 1 - \eta + \eta(P_{i,rad} + P_{i,nonrad})/P_0$ ($i = \parallel, \perp$). In the simulation, P_0, $P_{i,rad}$, and $P_{i,nonrad}$ are evaluated as the total dipole emission power into the homogeneous dielectric environment (PMMA), total dipole radiative power into the far field, and the dissipated power in the multilayer nanostructures, respectively.[11,17,34,43] To compare with emission rate enhancement obtained from photoluminescence decay measurements, dipole emitters at different heights away from the top surface of the multilayers and at different locations inside the multilayer grating grooves are considered in the simulations.

DOI: 10.1021/acsphotonics.6b01039
ACS Photonics 2017, 4, 501−508

Experimental Setup. QDs' spontaneous emission lifetime is measured by using a time-correlated single photon counting system (PicoQuant Photonics). A picosecond-pulsed excitation source is operated at an emission wavelength of 402 nm, minimum pulse width of 52 ps, repetition rate of 10 MHz, and mean excitation power of 0.25 μW measured at the entrance to an objective lens (NA 0.5). This objective lens was used to couple both excitation to and emission from the QDs. A single-photon counting module was synchronized with the pulsed excitation source to obtain the time-resolved photoluminescence intensity of the QD emission, by detecting the emission signals from an optical fiber mounted on the side exit slit of a spectrometer (Horiba IHR550). The QDs' emission spectra are obtained from a liquid N_2 cooled CCD detector.

Photoluminescence Decay Curve Fitting. The spontaneous emission lifetime of the QDs on the multilayer sample and glass substrate are obtained by fitting the experimental photoluminescence decay data using a modified exponential relaxation model:[30−33]

$$I(t) = I_0 e^{-(t/\tau)^{\beta}} + I_b \quad (5)$$

where τ is the decay lifetime after which the photoluminescence intensity $I(t)$ exponentially drops to $1/e$ of its initial value I_0. The modification parameter β describes the deviation of a realistic multiexponential photoluminescence decay measured in experiments from an ideal single-exponential decay model that recovers when $\beta = 1$. The stretched exponential relaxation model is a common choice to fit multicomponent exponential decays such as QD emission presented in this study.[30] Photoluminescence decay data within the full delay time limit (100 ns) are used in the curve fitting with eq 5. The fitted β values for the photoluminescence decay curves of QDs on a multilayer (glass) in Figure 2c are 1.10 (0.94) at 570 nm, 1.09 (0.94) at 600 nm, and 1.02 (0.97) at 650 nm. The fitted β values for QD decay curves on a multilayer grating (multilayer) in Figure 3a are 1.00 (1.07) at 620 nm and 0.98 (1.02) at 650 nm. The coefficients of determination (R-squared) for all these curve fittings are very close to 1 (ranging from 0.975 to 0.997), indicating the model (eq 5) fits all data very well. Berberan-Santos et al.[30] have proved that the ensemble average emission rate constant can be described as β/τ. Because all our fitted β values are very close to 1, the emission rate enhancement is obtained from the normalized fitted decay lifetime in the current study to demonstrate enhancement effects of the multilayer nanostructures for all possible QD emission channels.

■ ASSOCIATED CONTENT

Supporting Information

The Supporting Information is available free of charge on the ACS Publications website at DOI: 10.1021/acsphotonics.6b01039.

Details on the effective permittivity of a multilayer calculated with local and nonlocal EMT and the dependence of the Purcell factor on the Ag filling ratio of the multilayer (PDF)

■ AUTHOR INFORMATION

Corresponding Author

*E-mail: (J. Gao) gaojie@mst.edu.

ORCID

Ling Li: 0000-0003-2973-9848

Xiaodong Yang: 0000-0001-9031-3155

Jie Gao: 0000-0003-0772-4530

Author Contributions

The manuscript is written through contributions of all authors. All authors have given approval to the final version of the manuscript.

Notes

The authors declare no competing financial interest.

■ ACKNOWLEDGMENTS

The authors acknowledge the support from the National Science Foundation under grants ECCS-1653032, CBET-1402743, and DMR-1552871. This work was performed, in part, at the Center for Integrated Nanotechnologies, an Office of Science User Facility operated for the U.S. Department of Energy (DOE) Office of Science. Sandia National Laboratories is a multiprogram laboratory managed and operated by the Sandia Corporation, a wholly owned subsidiary of the Lockheed Martin Corporation, for the U.S. Department of Energy's National Nuclear Security Administration under contract DE-AC04-94AL85000.

■ REFERENCES

(1) Gao, J.; Sun, L.; Deng, H.; Mathai, C. J.; Gangopadhyay, S.; Yang, X. Experimental realization of epsilon-near-zero metamaterial slabs with metal-dielectric multilayers. *Appl. Phys. Lett.* **2013**, *103*, 051111.

(2) Maas, R.; Parsons, J.; Engheta, N.; Polman, A. Experimental realization of an epsilon-near-zero metamaterial at visible wavelengths. *Nat. Photonics* **2013**, *7*, 907−912.

(3) Poddubny, A.; Iorsh, I.; Belov, P.; Kivshar, Y. Hyperbolic metamaterials. *Nat. Photonics* **2013**, *7*, 948−957.

(4) Yang, X.; Hu, C.; Deng, H.; Rosenmann, D.; Czaplewski, D. A.; Gao, J. Experimental demonstration of near-infrared epsilon-near-zero multilayer metamaterial slabs. *Opt. Express* **2013**, *21*, 23631−23639.

(5) Shekhar, P.; Atkinson, J.; Jacob, Z. Hyperbolic metamaterials: fundamentals and applications. *Nano Convergence* **2014**, *1*, 1−17.

(6) Subramania, G.; Fischer, A.; Luk, T. Optical properties of metal-dielectric based epsilon near zero metamaterials. *Appl. Phys. Lett.* **2012**, *101*, 241107.

(7) Wood, B.; Pendry, J.; Tsai, D. Directed subwavelength imaging using a layered metal-dielectric system. *Phys. Rev. B: Condens. Matter Mater. Phys.* **2006**, *74*, 115116.

(8) Iorsh, I.; Poddubny, A.; Orlov, A.; Belov, P.; Kivshar, Y. S. Spontaneous emission enhancement in metal−dielectric metamaterials. *Phys. Lett. A* **2012**, *376*, 185−187.

(9) Jacob, Z.; Smolyaninov, I. I.; Narimanov, E. E. Broadband Purcell effect: Radiative decay engineering with metamaterials. *Appl. Phys. Lett.* **2012**, *100*, 181105.

(10) Kim, J.; Drachev, V. P.; Jacob, Z.; Naik, G. V.; Boltasseva, A.; Narimanov, E. E.; Shalaev, V. M. Improving the radiative decay rate for dye molecules with hyperbolic metamaterials. *Opt. Express* **2012**, *20*, 8100−8116.

(11) Krishnamoorthy, H. N.; Jacob, Z.; Narimanov, E.; Kretzschmar, I.; Menon, V. M. Topological transitions in metamaterials. *Science (Washington, DC, U. S.)* **2012**, *336*, 205−209.

(12) Newman, W. D.; Cortes, C. L.; Jacob, Z. Enhanced and directional single-photon emission in hyperbolic metamaterials. *J. Opt. Soc. Am. B* **2013**, *30*, 766−775.

(13) Sreekanth, K.; Biaglow, T.; Strangi, G. Directional spontaneous emission enhancement in hyperbolic metamaterials. *J. Appl. Phys. (Melville, NY, U. S.)* **2013**, *114*, 134306.

(14) Ferrari, L.; Lu, D.; Lepage, D.; Liu, Z. Enhanced spontaneous emission inside hyperbolic metamaterials. *Opt. Express* **2014**, *22*, 4301−4306.

(15) Galfsky, T.; Krishnamoorthy, H.; Newman, W.; Narimanov, E.; Jacob, Z.; Menon, V. Active hyperbolic metamaterials: enhanced spontaneous emission and light extraction. *Optica* **2015**, *2*, 62−65.
(16) Shalaginov, M. Y.; Ishii, S.; Liu, J.; Irudayaraj, J.; Lagutchev, A.; Kildishev, A. V.; Shalaev, V. M. Broadband enhancement of spontaneous emission from nitrogen-vacancy centers in nanodiamonds by hyperbolic metamaterials. *Appl. Phys. Lett.* **2013**, *102*, 173114.
(17) Lu, D.; Kan, J. J.; Fullerton, E. E.; Liu, Z. Enhancing spontaneous emission rates of molecules using nanopatterned multilayer hyperbolic metamaterials. *Nat. Nanotechnol.* **2014**, *9*, 48−53.
(18) Ferrari, L.; Wu, C.; Lepage, D.; Zhang, X.; Liu, Z. Hyperbolic metamaterials and their applications. *Prog. Quantum Electron.* **2014**, *40*, 1.
(19) Tomaš, M.-S.; Lenac, Z. Spontaneous-emission spectrum in an absorbing Fabry-Perot cavity. *Phys. Rev. A: At., Mol., Opt. Phys.* **1999**, *60*, 2431.
(20) Choy, J. T.; Hausmann, B. J.; Babinec, T. M.; Bulu, I.; Khan, M.; Maletinsky, P.; Yacoby, A.; Lončar, M. Enhanced single-photon emission from a diamond-silver aperture. *Nat. Photonics* **2011**, *5*, 738−743.
(21) Ozel, T.; Nizamoglu, S.; Sefunc, M. A.; Samarskaya, O.; Ozel, I. O.; Mutlugun, E.; Lesnyak, V.; Gaponik, N.; Eychmuller, A.; Gaponenko, S. V. Anisotropic emission from multilayered plasmon resonator nanocomposites of isotropic semiconductor quantum dots. *ACS Nano* **2011**, *5*, 1328−1334.
(22) Belacel, C.; Habert, B.; Bigourdan, F.; Marquier, F.; Hugonin, J.-P.; Michaelis de Vasconcellos, S.; Lafosse, X.; Coolen, L.; Schwob, C.; Javaux, C. Controlling spontaneous emission with plasmonic optical patch antennas. *Nano Lett.* **2013**, *13*, 1516−1521.
(23) Zhukovsky, S.; Ozel, T.; Mutlugun, E.; Gaponik, N.; Eychmuller, A.; Lavrinenko, A.; Demir, H.; Gaponenko, S. Hyperbolic metamaterials based on quantum-dot plasmon-resonator nanocomposites. *Opt. Express* **2014**, *22*, 18290−18298.
(24) Sreekanth, K. V.; Krishna, K. H.; De Luca, A.; Strangi, G. Large spontaneous emission rate enhancement in grating coupled hyperbolic metamaterials. *Sci. Rep.* **2014**, *4*.634010.1038/srep06340
(25) Sreekanth, K. V.; De Luca, A.; Strangi, G. Experimental demonstration of surface and bulk plasmon polaritons in hypergratings. *Sci. Rep.* **2013**, *3*.10.1038/srep03291
(26) Kidwai, O.; Zhukovsky, S. V.; Sipe, J. Dipole radiation near hyperbolic metamaterials: applicability of effective-medium approximation. *Opt. Lett.* **2011**, *36*, 2530−2532.
(27) Orlov, A. A.; Voroshilov, P. M.; Belov, P. A.; Kivshar, Y. S. Engineered optical nonlocality in nanostructured metamaterials. *Phys. Rev. B: Condens. Matter Mater. Phys.* **2011**, *84*, 045424.
(28) Kidwai, O.; Zhukovsky, S. V.; Sipe, J. Effective-medium approach to planar multilayer hyperbolic metamaterials: Strengths and limitations. *Phys. Rev. A: At., Mol., Opt. Phys.* **2012**, *85*, 053842.
(29) Sun, L.; Cheng, F.; Mathai, C. J.; Gangopadhyay, S.; Gao, J.; Yang, X. Experimental characterization of optical nonlocality in metal-dielectric multilayer metamaterials. *Opt. Express* **2014**, *22*, 22974−22980.
(30) Berberan-Santos, M.; Bodunov, E.; Valeur, B. Mathematical functions for the analysis of luminescence decays with underlying distributions 1. Kohlrausch decay function (stretched exponential). *Chem. Phys.* **2005**, *315*, 171−182.
(31) Schlegel, G.; Bohnenberger, J.; Potapova, I.; Mews, A. Fluorescence decay time of single semiconductor nanocrystals. *Phys. Rev. Lett.* **2002**, *88*, 137401.
(32) Lee, K. B.; Siegel, J.; Webb, S.; Leveque-Fort, S.; Cole, M.; Jones, R.; Dowling, K.; Lever, M.; French, P. Application of the stretched exponential function to fluorescence lifetime imaging. *Biophys. J.* **2001**, *81*, 1265−1274.
(33) Berberan-Santos, M. N. A luminescence decay function encompassing the stretched exponential and the compressed hyperbola. *Chem. Phys. Lett.* **2008**, *460*, 146−150.
(34) Ford, G. W.; Weber, W. H. Electromagnetic interactions of molecules with metal surfaces. *Phys. Rep.* **1984**, *113*, 195−287.
(35) Leistikow, M.; Johansen, J.; Kettelarij, A.; Lodahl, P.; Vos, W. Size-dependent oscillator strength and quantum efficiency of CdSe quantum dots controlled via the local density of states. *Phys. Rev. B: Condens. Matter Mater. Phys.* **2009**, *79*, 045301.
(36) Shalaginov, M. Y.; Vorobyov, V. V.; Liu, J.; Ferrera, M.; Akimov, A. V.; Lagutchev, A.; Smolyaninov, A. N.; Klimov, V. V.; Irudayaraj, J.; Kildishev, A. V. Enhancement of single-photon emission from nitrogen-vacancy centers with TiN/(Al, Sc) N hyperbolic metamaterial. *Laser Photonics Rev.* **2015**, *9*, 120−127.
(37) Le-Van, Q.; Le Roux, X.; Aassime, A.; Degiron, A. Electrically driven optical metamaterials. *Nat. Commun.* **2016**, *7*.1201710.1038/ncomms12017
(38) Oulton, R. F.; Sorger, V. J.; Zentgraf, T.; Ma, R.-M.; Gladden, C.; Dai, L.; Bartal, G.; Zhang, X. Plasmon lasers at deep subwavelength scale. *Nature (London, U. K.)* **2009**, *461*, 629−632.
(39) Meng, X.; Kildishev, A. V.; Fujita, K.; Tanaka, K.; Shalaev, V. M. Wavelength-tunable spasing in the visible. *Nano Lett.* **2013**, *13*, 4106−4112.
(40) Jin, X. R.; Sun, L.; Yang, X.; Gao, J. Quantum entanglement in plasmonic waveguides with near-zero mode indices. *Opt. Lett.* **2013**, *38*, 4078−4081.
(41) Jha, P. K.; Mrejen, M.; Kim, J.; Wu, C.; Wang, Y.; Rostovtsev, Y. V.; Zhang, X. Coherence-driven topological transition in quantum metamaterials. *Phys. Rev. Lett.* **2016**, *116*, 165502.
(42) Wylie, J.; Sipe, J. Quantum electrodynamics near an interface. II. *Phys. Rev. A: At., Mol., Opt. Phys.* **1985**, *32*, 2030.
(43) Barnes, W. Fluorescence near interfaces: the role of photonic mode density. *J. Mod. Opt.* **1998**, *45*, 661−699.

DOI: 10.1021/acsphotonics.6b01039
ACS Photonics 2017, 4, 501−508